Environmental Technology & Science Journal
Volume 17 Number 1 June 2026

Effect of Nano-Silica on Sodium Hydroxide Activated Blended Millet Husk Ash-Calcium Carbide Residue Concrete

[1]Abass A.I. & [2*]Ogunbode E.B.
[1]Department of Building Technology, Waziri Umaru Federal Polytechnic, Birnin Kebbi
[2]Department of Building, Federal University of Technology, Minna
[*]Corresponding author: ezekiel@futminna.edu.ng

Received: 24/03/2026 **Revised:** 8/04/2026 **Accepted:** 24/04/2026

The production of Portland cement is associated with high energy consumption and significant carbon dioxide (CO_2) emissions, necessitating sustainable alternative binders. This study investigates the effect of nano-silica (NS) on the fresh and mechanical properties of sodium hydroxide (NaOH)-activated blended Millet Husk Ash--Calcium Carbide Residue (MHA-CCR) concrete. Nano-silica was extracted in-house from MHA via a sol-gel chemical precipitation method. A four-factor Central Composite Design (CCD) was employed, varying MHA content (55-65%), CCR content (30-45%), NS dosage (3-6%), and NaOH molarity (8-12M) across 30 experimental runs. Slump, setting time, density, compressive strength, and splitting tensile strength were evaluated at 7, 14, 28, and 56 days. Increasing NaOH molarity and NS dosage reduced workability and accelerated setting, although slump remained above 45 mm for most activated mixes. NS incorporation improved density, compressive strength, and splitting tensile strength through enhanced matrix densification and cohesion. At 28 and 56 days, the MHA-CCR-NS system achieved compressive strengths of 41 N/mm² and 50 N/mm², respectively, equivalent to approximately 87% and 82% of the OPC control at the same ages. CCD optimization identified an optimal mix of 61.5% MHA, 34% CCR, 4% NS, and 11 M NaOH, with a predicted 28-day compressive strength of 41.86 N/mm². A desirability value of 1.0 indicates that the imposed response constraints are optimally satisfied within the experimental design space. These findings demonstrate the technical feasibility of producing structurally viable, low-carbon alkali-activated concrete from locally available agro-industrial wastes. Further studies are recommended to evaluate long-term durability and field performance.

Keywords: Alkali-activated concrete; NaOH-activated; Millet husk ash; Calcium carbide residue; Nano-silica; Ambient curing; Central Composite Design; Sustainable construction

Introduction

Concrete is the most widely used construction material due to its versatility, material availability, and structural applicability. However, Portland cement (PC), its conventional binder, contributes approximately 7-8% of global anthropogenic CO_2 emissions through energy-intensive clinker production (Andrew, 2018). Resource depletion and waste generation further challenge the sustainability of cement-based construction, necessitating low-carbon alternatives. Alkali-activated materials (AAMs) have emerged as promising substitutes, formed through alkaline activation of aluminosilicate-rich precursors to produce binders with favourable mechanical and durability properties (Provis, 2018). Recent research increasingly focuses on calcium-containing hybrid systems for improved ambient curing and early-age strength.

Unlike rice husk ash-lime systems, which rely on free-lime pozzolanic reactions (Kaze *et al*., 2021), and CCR-modified fly ash geopolymers, which benefit from industrial-quality aluminosilicate precursors (Bernal et al., 2011; Provis, 2018), the present MHA-CCR system uniquely combines a siliceous agro-ash precursor with a calcium-rich industrial residue under NaOH-only activation, without sodium silicate or industrial slag. To the best of current knowledge, this specific configuration has not been systematically optimized in open literature, constituting the primary knowledge gap addressed herein. Nano-silica (NS) has gained attention in AAM systems due to its ultra-fine size, high surface area, and amorphous reactivity. It enhances gel nucleation, pore refinement, and mechanical performance at low dosages (Tobie *et al*., 2021), though excessive content may reduce workability and increase brittleness. Unlike previous studies on rice husk ash-lime systems (Kaze *et al*., 2021) and CCR-modified fly ash geopolymers (Bernal *et al*., 2011), which rely on either free-lime pozzolanic reactions or industrial-quality aluminosilicate precursors, the present MHA-CCR-NS system uniquely combines a siliceous agro-ash precursor with a calcium-rich industrial residue under NaOH-only activation, without sodium silicate or elevated temperature curing.

This study addresses these gaps by characterising the MHA-CCR-NS system using SEM, EDS, and XRF, extracting NS from MHA via sol-gel synthesis, and applying CCD for multi-variable optimization of performance and workability.

Literature Review

This study is grounded in alkali-activation chemistry and damage mechanics theory, which explain the formation, mechanical behaviour, and failure of NaOH-activated MHA–CCR concrete. Alkali

activation involves dissolution and polycondensation of aluminosilicates into N-A-S-H and hybrid C-A-S-H/N-A-S-H gels (Provis, 2018; Luukkonen *et al*., 2018). Nano-silica enhances this process by providing nucleation sites, densifying the matrix, and refining pore structure, thereby improving strength and durability (Tobie et al., 2021).

Recent research on alkali-activated materials increasingly focuses on calcium-containing hybrid systems due to their improved ambient curing performance. Calcium promotes the coexistence of C-A-S-H and N-A-S-H gels, resulting in enhanced strength and reduced porosity (Bernal et al., 2011). In this regard, MHA–CCR represents a sustainable hybrid precursor system derived from locally available waste materials.

Sodium hydroxide is widely used as an activator due to its strong dissolution capacity for aluminosilicates (Provis & van Deventer, 2014). Although sodium silicate can accelerate reaction kinetics, NaOH-only systems remain effective, particularly in the presence of calcium-rich precursors such as CCR (Nath & Sarker, 2014).

Nano-silica typically improves performance at dosages of 1-6%, beyond which agglomeration may reduce workability (Tobie et al., 2021). Response Surface Methodology and Central Composite Design are applied to optimise interactions among precursor ratio, NaOH concentration, and nano-silica content (Montgomery, 2017).

Materials and Methods

Materials

Millet husk ash (MHA) was produced by washing, air-drying, and calcining millet husks at 700 °C to preserve amorphous silica and remove organics, consistent with pozzolanic practice (ASTM C618; Rangan, 2014). The ash was ground and sieved to 75 µm. Calcium carbide residue (CCR) was sourced was sourced from an acetylene gas production facility, oven-dried, pulverized, and sieved to 75 µm (ASTM C618, 2023). Both precursors were characterized using XRF and SEM/EDS.

Nano-silica (NS) was extracted in-house from MHA using a sol–gel chemical precipitation method adapted from Harun *et al*. (2024) and Fusinato *et al*. (2023), who demonstrated this alkaline dissolution-acid precipitation route for silica-rich agricultural ash. The core sequence adopted comprised: NaOH dissolution of pre-treated MHA at elevated temperature; filtration to remove insoluble residues; controlled addition of 2 M hydrochloric acid to pH ≈ 7 to precipitate silica gel; aging (24 h); washing with deionized water; and oven-drying at 105 °C. The calcination step at 700 °C for 3 h was added to reduce loss on ignition (LOI), consistent with ASTM C311/C311M-22 (2022). Equation 1 presents the key extraction reaction:

$$S_iO_2 + 2N_aOH \rightarrow N_aS_iO_3 + H_2O \quad (1)$$

This sodium silicate (Na_2SiO_3) is an intermediate product formed transiently during the extraction of nano-silica from MHA and is not externally added as an activator. The final nano-silica precipitate is washed and dried to remove residual alkali, ensuring that the NaOH-only activation of the MHA-CCR binder system contains no deliberately added sodium silicate.

The sol-gel extraction procedure yielded approximately 18.5 g of nano-silica per 100 g of raw MHA, corresponding to a yield of 18.5% by mass. While detailed particle size analysis (DLS/TEM) was beyond the scope of this study, the extracted material exhibited the characteristic white, low-density powder morphology and high amorphous SiO_2 content (96.8%, Table 2) consistent with nano-silica produced via sol-gel methods from agricultural ashes (Harun *et al*., 2024; Fusinato *et al*., 2023). The observed enhancement in mechanical properties (Section 4.3) further supports the nanoscale reactivity of the extracted material.

NaOH-only activation was adopted as a deliberate methodological choice to avoid sodium silicate's higher cost, supply chain dependency, and embodied carbon burden. The $Ca(OH)_2$-rich CCR partially compensates for the absence of sodium silicate by promoting C-A-S-H gel formation under ambient curing, consistent with Bernal *et al*. (2011).

Natural river sand and 10 mm crushed granite conforming to ASTM C33/C33M (2023) were used. NaOH solutions were prepared at varying molarities (8–12 M) from analytical-grade pellets, cooled to room temperature, per ASTM E291 (2019) and ASTM E200 (2020). The NaOH solution served as the sole liquid phase in AAM mixes. Mixing water for the OPC control met BS EN 1008:2002 requirements.

Material characterization

Specific gravity of all binder materials and aggregates was determined by the pycnometer method. Particle size distribution of aggregates was established by dry sieve analysis in accordance with ASTM C136/C136M. Coarse aggregate water absorption was below 1%, indicating minimal interference with activator concentration. XRF analysis quantified the oxide composition of MHA and CCR and SEM/EDS confirmed morphological and elemental characteristics relevant to alkali activation.

Table 1 presents specific gravity values and Table 2 summarizes the XRF oxide composition of the binder materials.

Table 1: Specific Gravity of Constituent Materials

Material	Average Specific Gravity
MHA	2.50
CCR	2.45
Nano-Silica (NS)	2.25
Fine Aggregate	2.63
Coarse Aggregate	2.75
OPC (Control)	3.10

Table 2: XRF Oxide Composition of Binder Materials

Properties	Constituent Materials		
	MHA	CCR	NS
SiO_2	72.3	21.4	96.80
AI_2O_3	3.46	3.02	0.85
Fe_2O_3	1.76	2.50	0.45
MnO	0.70	0.65	0.03
CaO	4.64	54.32	0.60
P_2O_5	6.10	4.90	0.35
K_2O	6.04	6.85	0.50
TiO_2	0.24	0.33	0.12
SO_3	0.22	0.26	0.05
Na_2O	1.23	8.73	0.15

SEM analysis of MHA (Figure 1a) at 10,000× magnification under low vacuum conditions (70 Pa, 20 kV, 10.2 mm working distance) revealed heterogeneous, irregular, and angular particles with fibrous surface texture, consistent with a reactive aluminosilicate precursor providing abundant contact points for alkali dissolution. EDS confirmed silicon as the dominant element (53.0 wt%), with oxygen (20.2 wt%) and minor calcium (1.30 wt%), consistent with the XRF SiO_2 content of 72.3 wt%. SEM analysis of CCR (Figure 1b) at 9,000× magnification (70 Pa, 20 kV, 6.9 mm working distance) revealed a highly porous, three-dimensional reticulated framework of thin-walled, plate-like agglomerates with hierarchical porosity and localised pore-wall collapse, characteristic of calcium hydroxide-dominated materials. EDS confirmed calcium as the dominant element (60.20 wt%), consistent with the XRF CaO content of 54.32 wt%, validating CCR as the principal calcium source.

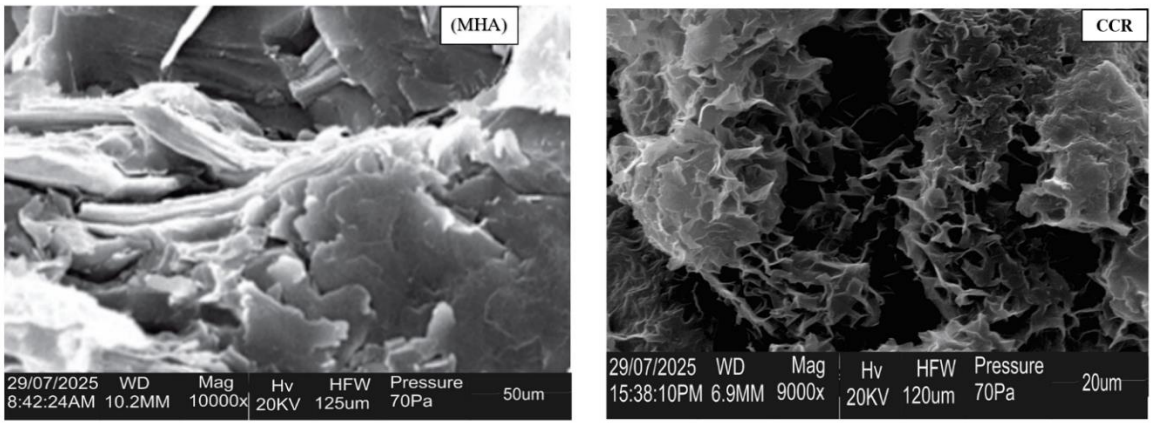

(a) **(b)**

Figure 1: Scanning Electron Microscopy (SEM) micrographs of (a) Millet Husk Ash (MHA) and (b) Calcium Carbide Residue (CCR), showing particle morphology, surface texture, and microstructural characteristics relevant to their pozzolanic and cementitious behaviour

Mix design and proportioning

A Portland cement control mix was designed using the Design of Experiments (DOE) approach with a target 28-day compressive strength of 43 N/mm² and water-cement ratio of 0.45. The control mix proportions per m³ were: Cement 456 kg, Fine Aggregate 792 kg, Coarse Aggregate 967 kg and Water 205 kg.

For the alkali-activated concrete, the total binder mass was maintained equal to the PC content (456 kg/m³). Individual binder quantities were: MHA 274 kg/m³ (60%), CCR 160 kg/m³ (35%) and NS 22 kg/m³ (5%). The NaOH solution (205 kg/m³) replaced mixing water in a 1:1 volumetric substitution. Table 3 summarizes the AAC mix design.

Table 3: Alkaline-Activated Concrete (AAC) Mix Design Per m³

Component	Quantity (kg/m³)
Millet Husk Ash (MHA)	274
Calcium Carbide Residue (CCR)	160
Nano-Silica (NS)	22
NaOH Solution (10 M)	205
Fine Aggregate	792
Coarse Aggregate	967
Total	2,420

Central composite design (CCD) and experimental optimization

A four-factor Central Composite Design (CCD) under Response Surface Methodology (RSM) was employed using Design-Expert software to explore multi-variable interaction effects. The four independent variables were: A = MHA content (55-65%), B = CCR content (30-45%), C = NS dosage (3-6%), and D = NaOH molarity (8-12 M). The NS upper limit of 6% was based on preliminary trials, which showed that dosages above 6% caused agglomeration and unworkable mixes (slump < 30 mm), consistent with Tobie *et al*. (2021). The NaOH range of 8–12 M was selected to balance dissolution efficiency with practical workability. Three response variables were modelled: slump (mm), initial setting time (min) and 28-day compressive strength (N/mm²).

The CCD comprised 16 factorial points, 8 axial points and 6 centre points, totalling 30 experimental runs. Equation 2 presents a quadratic polynomial model of the following form was fitted to each response:

$$\gamma = \beta_0 + \sum \beta_i x_i + \sum\sum \beta_{ij} x_i x_j + \sum \beta_{ij} x_i^2 \quad (2)$$

where Y is the response, x_i and x_j are coded variables and β represents regression coefficients. The model adequacy was assessed by ANOVA, R^2 values and lack-of-fit tests. Multi-objective desirability function optimization was used to identify optimal mix proportions simultaneously maximizing strength and workability.

Specimen casting, curing and testing

All test procedures in this study followed ASTM and BS EN standards originally developed for Portland cement systems, as no universally accepted standards currently exist for alkali-activated materials (AAMs). This approach is consistent with established practice in AAM research (Provis & van Deventer, 2014; Bernal *et al*., 2011) and enables direct comparative evaluation against OPC control concrete. However, the following adaptations were made to account for the distinct reaction kinetics of NaOH-activated binders: (i) setting time was determined using the Vicat needle apparatus (ASTM C191-21), with initial and final setting defined as the time to reach 25 mm and 0 mm penetration, respectively, recognising that AAM pastes may exhibit different penetration-depth relationships than OPC; (ii) slump testing (BS EN 12350-2:2019) was performed immediately after mixing completion, without delay, to capture the rapid stiffening characteristic of high-molarity NaOH systems; (iii) all specimens were cured at ambient temperature (27 ± 2 °C) without elevated-temperature curing, as standardised accelerated curing protocols for AAMs (e.g., 60–80 °C) would not reflect practical field applications in tropical developing contexts. Despite these adaptations, the comparative validity of the results remains sound, as the same procedures were applied consistently across all mixes, including the OPC control.

Specimens were cast in 100 × 100 × 100 mm cube moulds for compressive strength and density tests and 100 mm × 200 mm cylinder moulds for splitting tensile strength. All mixes were cured at ambient temperature (approximately 27 ± 2 °C) without steam or elevated temperature curing, to reflect practical field conditions. Testing was conducted at 7, 14, 28 and 56 days of curing.

Fresh properties were evaluated using slump (BS EN 12350-2:2019) and setting time (ASTM C191-21, adapted for non-Portland cement binders). Density was determined in accordance with ASTM C642, while compressive strength and splitting tensile strength were tested using BS EN 12390-3:2019 and ASTM C496/C496M (2017), respectively. Although these standards were originally developed for Portland cement systems, their application to alkali-activated materials is consistent with established comparative practice in the literature (Provis & van Deventer, 2014). ASTM C618 was used only for preliminary screening purposes, without implying formal classification of the materials.

Results and Discussion

Fresh properties: workability and setting time

Table 4 presents the slump and setting time results for the 30 CCD runs Slump values ranged from 38 to 78 mm, with the majority of activated mixes maintaining workability above 45 mm, except for high NaOH (12

M) and high NS (6%) combinations (e.g., Run 15: 38 mm). A clear inverse relationship was observed between NaOH molarity and slump, attributable to accelerated aluminosilicate dissolution, rapid gel nucleation, and increased activator solution viscosity (Temuujin et al., 2011; Mohamed et al., 2024). Nano-silica further reduced workability through particle agglomeration and increased water demand. Although sodium silicate-based activators generally induce more severe fresh-state stiffening due to their additional soluble silica content (Provis & van Deventer, 2014; Nath & Sarker, 2014), the NaOH-only system employed herein maintained workable consistency while supporting effective polycondensation through internally supplied calcium and silica from CCR and MHA.

Setting time was similarly governed by activator concentration, with increasing NaOH molarity from 8 M to 12 M reducing final setting time from approximately 420 to 280 min. This behaviour is attributed to increased OH^- concentration, which enhances dissolution of reactive SiO_2 and Al_2O_3 species from MHA (Provis, 2018; Mohamed *et al*., 2024). Nano-silica exerted a dual influence: slight retardation of initial setting due to water adsorption at early stages, followed by accelerated final setting through provision of nucleation sites for gel growth (Tobie *et al.*, 2021). The observed inverse relationship between slump and setting time confirms that activator-driven reaction kinetics simultaneously govern both fresh properties, underscoring the importance of jointly optimising NaOH molarity and NS dosage.

Table 4: Fresh properties and 28-day compressive strength of MHA-CCR-NS concrete for all CCD runs

Run	Type	MHA (%)	CCR (%)	NS (%)	NaOH (M)	Slump (mm)	Compressive Strength @ 28d (N/mm^2)
1	Factorial	55	30	3	8	72	40.2
2	Factorial	65	30	3	8	76	39.7
3	Factorial	55	45	3	8	70	38.8
4	Factorial	65	45	3	8	74	39.6
5	Factorial	55	30	6	8	66	40.6
6	Factorial	65	30	6	8	70	42.5
7	Factorial	55	45	6	8	64	40.5
8	Factorial	65	45	6	8	68	42.7
9	Factorial	55	30	3	12	46	42.2
10	Factorial	65	30	3	12	50	42.7
11	Factorial	55	45	3	12	44	43
12	Factorial	65	45	3	12	48	42.6
13	Factorial	55	30	6	12	40	43.6
14	Factorial	65	30	6	12	44	44.8
15	Factorial	55	45	6	12	38	43.5
16	Factorial	65	45	6	12	42	44.9
17	Axial	50	37.5	4.5	10	59	41
18	Axial	70	37.5	4.5	10	63	42.6
19	Axial	60	22.5	4.5	10	62	43.1
20	Axial	60	52.5	4.5	10	58	42.9
21	Axial	60	37.5	1.5	10	66	41
22	Axial	60	37.5	7.5	10	54	44.5
23	Axial	60	37.5	4.5	6	78	39
24	Axial	60	37.5	4.5	14	38	42.4
25	Centre	60	37.5	4.5	10	60	42.5
26	Centre	60	37.5	4.5	10	61	41.9
27	Centre	60	37.5	4.5	10	59	42.4
28	Centre	60	37.5	4.5	10	60	41.8
29	Centre	60	37.5	4.5	10	61	42.6
30	Centre	60	37.5	4.5	10	60	42

Density development

Density determination followed ASTM C642, which assumes water absorption as an indicator of capillary porosity. While AAMs may exhibit different pore structure characteristics (e.g., finer gel pores vs. capillary pores), the standard remains valid for comparative density measurement between OPC and AAM specimens, as the same saturation and boiling procedures were applied uniformly.

Figure 2 presents the average density of cube and cylindrical MHA-CCR-NS concrete specimens at each curing age. Density increased progressively with curing, reflecting ongoing geopolymerization, gel precipitation and pore refinement characteristic of alkali-activated systems (Shi *et al*., 2017). Cube specimens consistently recorded slightly higher densities than cylinders at corresponding ages, attributable to specimen geometry and compaction efficiency rather than material inconsistency.

The 28-day cube density of 2277 kg/m³ represents a 1.4% increase over the 7-day value, aligning with peak compressive strength development. The steady density rise from 7 to 56 days indicates progressive gel maturation and matrix densification, partly attributed to the nano-filling effect of nano-silica within the pore structure (Tobie *et al*., 2021).

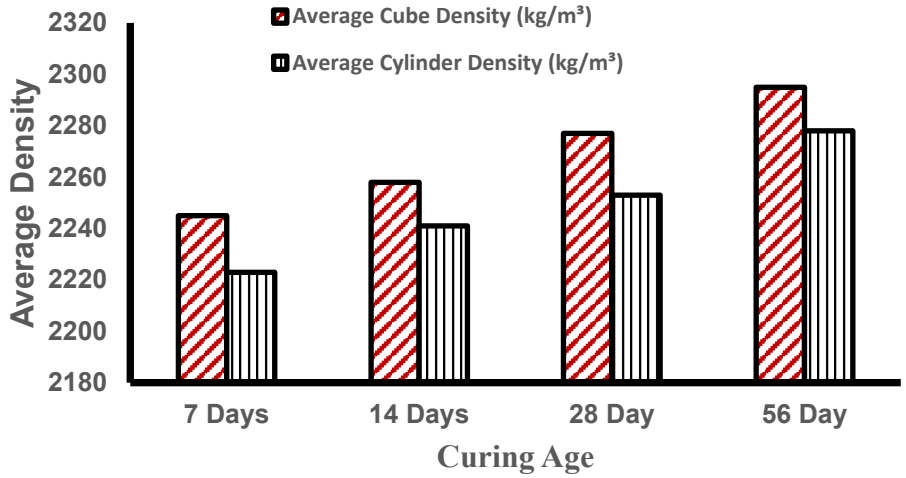

Figure 2: Average density of MHA-CCR-NS concrete at different curing ages, showing the influence of hydration progress and material interactions on bulk density development

Compressive strength

Table 4 and Figure 3 present compressive strength data for both control and MHA-CCR-NS concrete across all curing ages. The OPC control followed the typical strength development trajectory, reaching 23 N/mm² at 7 days, 26 N/mm² at 14 days, 47 N/mm² at 28 days and 61 N/mm² at 56 days.

The MHA-CCR-NS concrete achieved 16 N/mm² at 7 days, indicating initiation of alkali-activation reactions. The calcium from CCR contributed to early C-A-S-H gel formation, while NS facilitated nucleation effects. By 28 days, compressive strength reached 41 N/mm², achieving approximately 87% of the OPC control. At 56 days, strength further increased to 50 N/mm² (82% of control), confirming sustained long-term gel maturation. The deceleration of strength gain beyond 28 days is characteristic of NaOH-only activated systems, where the primary dissolution and polycondensation reactions are substantially complete by 28 days (Provis, 2018; Bernal et al., 2011). The competitive early-age performance confirms that CCR calcium was sufficient to initiate C-A-S-H nucleation under ambient conditions without elevated temperature curing.

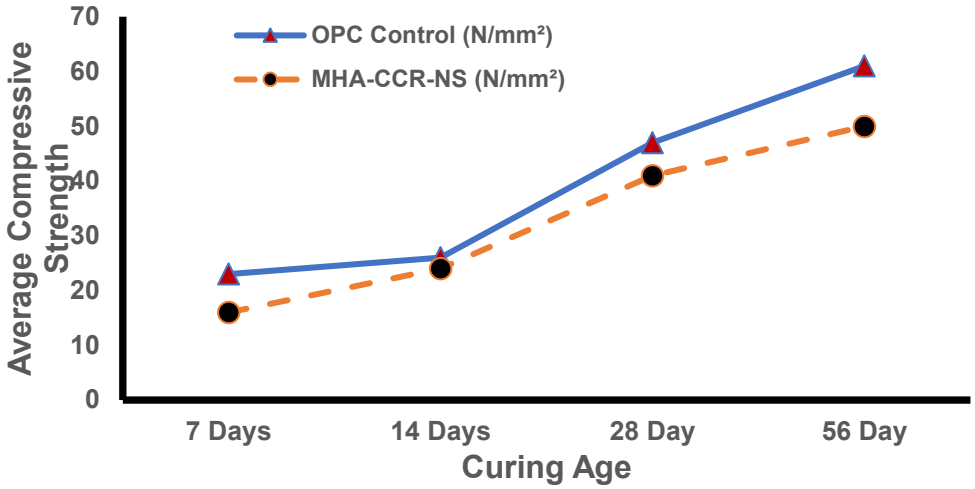

Figure 3: Compressive strength comparison between Ordinary Portland Cement (OPC) control concrete and MHA–CCR–NS blended concrete, illustrating the influence of supplementary materials on strength development

CCD Optimization and response surface analysis

ANOVA for the 28-day compressive strength model is summarized in Table 5. The model was highly significant ($p < 0.0001$) and the non-significant lack-of-fit ($F = 2.42$, $p = 0.1708$) confirms model reliability for prediction.

NaOH molarity (D) was the dominant factor ($F = 160.64$, $p < 0.0001$), followed by NS dosage (C) ($F = 83.75$, $p < 0.0001$) and MHA content (A) ($F = 19.58$, $p = 0.0005$). Statistical analysis revealed that CCR content significantly influenced 28-day compressive strength ($p = 0.0433$, Table 5). This confirms that calcium derived from CCR (54.3% CaO, Table 2) contributes to C-A-S-H gel formation under NaOH-only activation. The significant AC interaction (MHA × NS, $p = 0.0047$) reflects synergistic coupling between MHA silica availability and NS nucleation efficacy: higher MHA content increases dissolved silicate species available for NS-induced heterogeneous nucleation, promoting denser N-A-S-H gel growth. The significant D^2 term ($p = 0.0007$) confirms a non-linear optimum for NaOH concentration, beyond which excessive acceleration leads to workability loss without proportional strength benefit.

The regression model (Equation 3) provided the quadratic relationship between the four factors and 28-day compressive strength:

$$\mathbf{CS(28d)} = \beta_0 + \beta_1 A + \beta_2 B + \beta_3 C + \beta_4 D + \beta_{12} AB + \beta_{13} AC + \beta_{14} AD + \beta_{23} BC + \beta_{24} BD + \beta_{34} CD + \beta_{11} A^2 + \beta_{22} B^2 + \beta_{33} C^2 + \beta_{44} D^2 \quad (3)$$

Table 5: ANOVA Summary for 28-Day Compressive Strength Model

Source	Sum of Squares	df	Mean Square	F-Value	p-Value	Significance
Model	69.57	14	4.97	22.01	< 0.0001	Significant
A – MHA	4.42	1	4.42	19.58	0.0005	
B – CCR	1.024	1	1.024	4.54	0.0433	
C – NS	18.90	1	18.90	83.75	< 0.0001	
D – NaOH	36.26	1	36.26	160.64	< 0.0001	
AC	2.48	1	2.48	10.99	0.0047	
D^2	4.10	1	4.10	18.15	0.0007	
Residual	3.39	15	0.2257	—	—	
Lack of Fit	2.81	10	0.2806	2.42	0.1708	Not Significant
Cor Total	72.95	29	—	—	—	

Note: $R^2 = 0.954$, Adjusted $R^2 = 0.911$

The 3D response surface plot (Figure 4) provides compelling visual evidence of a positive and relatively stable relationship between the studied factors and compressive strength. The smooth, ascending surface geometry confirms the adequacy of the fitted quadratic RSM model and supports the reliability of the optimization results. The findings suggest that increasing MHA content within the studied range consistently enhances compressive strength, while CCR contributes modestly, particularly at higher combination levels. Together, these insights validate the selected optimal mix proportions for achieving target mechanical performance.

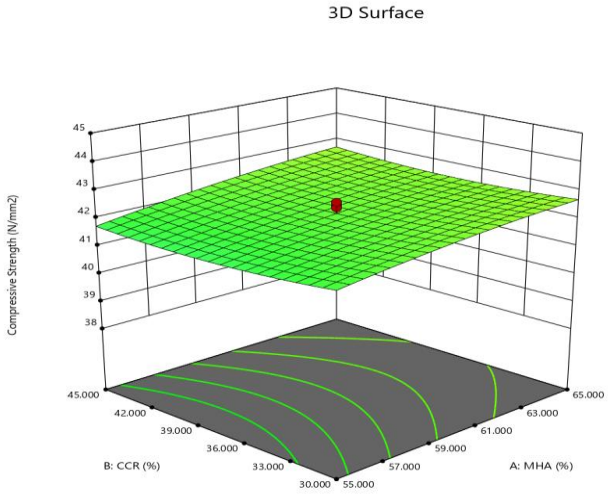

Figure 4: Three-dimensional response surface plot illustrating the combined effect of Millet Husk Ash (MHA) and Calcium Carbide Residue (CCR) replacement levels on the compressive strength (N/mm²) of concrete

The Predicted vs. Actual plot (Figure 5) confirms that the RSM model developed in this study is statistically adequate and experimentally reliable for predicting compressive strength as a function of MHA and CCR content. The strong agreement between predicted and actual values across the full experimental range lends credibility to the optimization results and the recommended optimal mix proportions identified in the study.

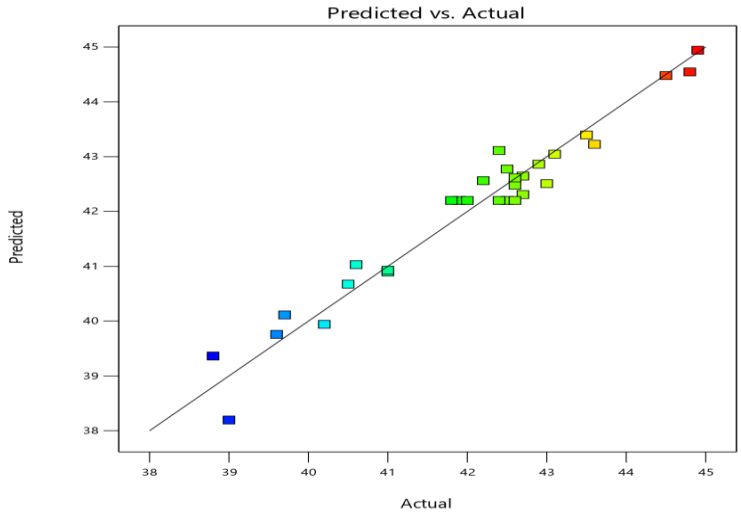

Figure 5: Predicted vs. Actual Plot Showing the Adequacy of the Fitted Quadratic Model for Compressive Strength (N/mm²)

The combined analysis of both plots (Figure 6) indicates that the optimal mix for maximum desirability and high compressive strength occurs at approximately MHA 61%, CCR 34% and NS 4%, This region satisfies all constraints with a desirability of 1 and predicts a compressive strength of about 41.87 N/mm², confirming the effectiveness of the RSM optimization approach.

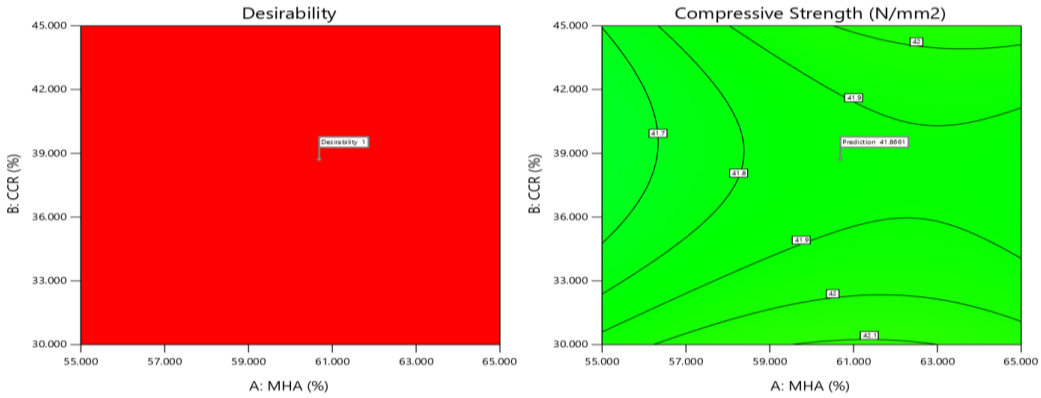

Figure 6: Contour plots of desirability (left) and compressive strength (right), showing the optimization domain for MHA and CCR replacement levels based on response surface methodology

Optimization using desirability function

Multi-objective desirability optimisation identified an optimal mix of 61.5% MHA, 34% CCR, 4% NS, and 11 M NaOH, producing a predicted 28-day compressive strength of 41.86 N/mm², slump of 60 mm, and desirability of 1.0. The result reflects a balance between activator-driven reaction intensity and workability preservation, confirming non-linear multi-variable interactions in alkali-activated systems. The desirability value of 1.0 reflects optimization within the experimental design space and should not be interpreted as a direct performance guarantee under field conditions. Centre-point replicates (Runs 25–30) recorded compressive strength values between 41.8 and 42.6 N/mm², indicating a minor experimental variation of approximately ±0.4 N/mm² around the predicted response. Variability in the amorphous silica content of MHA and the calcium hydroxide composition of CCR may introduce natural fluctuations in response behaviour; therefore, quality control of precursor materials is recommended during scale-up applications.

Table 6: Optimized Mix Proportions (CCD)

Parameter	Optimal Value
MHA (%)	61.5
CCR (%)	34
NS (%)	4
NaOH (M)	11
Predicted Compressive Strength (N/mm^2)	**41.86**
Desirability	1.0
Slump	60 mm

Conclusion

The findings are based on laboratory scale experiments conducted under controlled ambient curing conditions (27 ± 2 °C) and should therefore be interpreted with caution when extrapolating to field scale applications.

This study demonstrates that NaOH-activated concrete incorporating Millet Husk Ash (MHA), Calcium Carbide Residue (CCR), and nano-silica (NS) can achieve structural-grade performance under ambient curing conditions without the need for sodium silicate. The developed system attained compressive strengths of 41 N/mm² and 50 N/mm² at 28 and 56 days, corresponding to 87% and 82% of OPC control, alongside comparable tensile performance, confirming its suitability for C30-C35 applications. However, increased NaOH molarity and nano-silica dosage reduced workability and accelerated setting, indicating the need for careful mix design balance.

Statistical optimization using Central Composite Design identified NaOH molarity and nano-silica dosage as the dominant factors, with CCR content also significantly influencing 28-day compressive strength ($p = 0.0433$). The significant MHA–NS interaction ($p = 0.0047$) and non-linear NaOH optimum ($p = 0.0007$) confirm the complex multi-variable interactions governing this sodium silicate-free alkali-activated system. The optimal composition (61.5% MHA, 34% CCR, 4% NS, 11 M NaOH) yielded a predicted compressive strength of 41.86 N/mm² with maximum desirability (1.0). These findings establish a viable pathway for sodium silicate-free alkali activation, contributing to the development of low-carbon

concrete using locally available agro-industrial waste materials.

Based on typical emission factors for OPC (~930 kg CO_2/tonne, Andrew 2018) and the elimination of clinker calcination in the proposed binder, the MHA-CCR-NS system is expected to achieve substantial direct CO_2 emissions reduction. Preliminary estimates using literature values for NaOH production (~1.5 kg CO_2/kg NaOH) suggest a reduction on the order of 60-75%, though a full life cycle assessment (LCA) is required to confirm net savings including activator production and precursor transport.

This study is subject to several limitations; microstructural characterization was limited to SEM/EDS; XRD and FTIR analyses would provide deeper insight into gel phase assemblage and the balance between N-A-S-H and C-A-S-H phases; all experiments were conducted at laboratory scale under controlled ambient curing (27 ± 2 °C); field-scale performance under variable conditions requires further investigation; long-term durability performance carbonation resistance, sulphate attack, shrinkage, creep, freeze-thaw and acid attack was not assessed and constitutes the primary direction for future research.

While a full life cycle assessment is beyond the scope of this study, the substantial reduction in clinker-derived emissions positions the MHA-CCR-NS system as a promising low-carbon alternative to OPC for structural applications. Future work should focus on durability performance, microstructural validation (XRD, FTIR), hybrid activator systems, and field-scale implementation to support practical adoption.

References

Andrew, R. M. (2018). Global CO_2 emissions from cement production. *Earth System Science Data, 10*(1), 195–217. https://doi.org/10.5194/essd-10-195-2018

ASTM C33/C33M. (2023). *Standard specification for concrete aggregates*. ASTM International.

ASTM C136/C136M. (2023). *Standard test method for sieve analysis of fine and coarse aggregates*. ASTM International.

ASTM C191-21. (2021). *Standard test methods for time of setting of hydraulic cement by Vicat needle*. ASTM International.

ASTM C311/C311M-22. (2022). *Standard test methods for sampling and testing fly ash or natural pozzolans for use in Portland-cement concrete*. ASTM International. https://doi.org/10.1520/C0311_C0311M-22

ASTM C496/C496M. (2017). *Standard test method for splitting tensile strength of cylindrical concrete specimens*. ASTM International.

ASTM C618. (2023). *Standard specification for coal fly ash and raw or calcined natural pozzolan for use in concrete*. ASTM International.

ASTM International. (2021). *ASTM C642-21: Standard test method for density, absorption, and voids in hardened concrete*. ASTM International

ASTM E200. (2020). *Standard practice for preparation, standardization, and storage of standard and reagent solutions for chemical analysis*. ASTM International.

ASTM E291. (2019). *Standard test methods for chemical analysis of caustic soda and caustic potash (sodium hydroxide and potassium hydroxide)*. ASTM International.

Bernal, S. A., Provis, J. L., Walkley, B., San Nicolas, R., Gehman, J. D., Brice, D. G., Kilcullen, A. R., Duxson, P., & van Deventer, J. S. J. (2011). Gel nanostructure in alkali-activated binders based on slag and fly ash and effects of accelerated carbonation. *Cement and Concrete Research, 41*(4), 412-420. https://doi.org/10.1016/j.cemconres.2011.02.010

British Standards Institution. (2002). *BS EN 1008:2002: Mixing water for concrete. British Standards Institution.*

BS EN 12350-2. (2019). *Testing fresh concrete - Part 2: Slump test*. British Standards Institution.

BS EN 12390-3. (2019). *Testing hardened concrete - Part 3: Compressive strength of test specimens*. British Standards Institution.

Fusinato, M. D., da Silva Amaral, M. A. F., de Irigon, P. I., Calgaro, C. O., de Los Santos, D. G., & Filho, P. J. S. (2023). Silica extraction from rice hull ash through the sol-gel process under ultrasound. *Environmental Science and Pollution Research, 30*(8), 21494-21511.

Harun, Z., Azhar, F. H., Hussin, R., Ibrahim, S. A., Hubadillah, S. K., & Sazali, N. (2024). The extraction of organic silica from agricultural waste: A mini review. *Emerging Advances in Integrated Technology, 5*(1), 65-74.

Kaze, C. R., Adesina, A., Lecomte-Nana, G. L., Metekong, J. V. S., Samen, L. V. E. K., Kamseu, E., & Melo, U. C. (2021). Synergetic effect of rice husk ash and quartz sand on microstructural and physical properties of laterite clay-based geopolymer. *Journal of Building Engineering, 43*, 103229.

Luukkonen, T., Abdollahnejad, Z., Yliniemi, J., Kinnunen, P., & Illikainen, M. (2018). One-part alkali-activated materials: A review. *Cement and Concrete Research, 103*, 21–34.

Mohamed, O. A., Najm, O., Zuaiter, H. A., Saleem, S. K., Ivak, S., & Al-Aribe, K. (2024). Effect of activator concentration on setting time, workability and compressive strength of sustainable concrete with alkali-activated slag binder. *Materials Today: Proceedings*.

Montgomery, D. C. (2017). *Design and analysis of experiments* (9th ed.). John Wiley & Sons.

Nath, P., & Sarker, P. K. (2014). Effect of NaOH concentration on strength and durability of geopolymer concrete. *Construction and Building Materials, 55*, 163-170.

Neville, A. M. (2011). *Properties of concrete* (5th ed.). Pearson Education Limited.

Provis, J. L. (2018). Alkali-activated materials. *Cement and Concrete Research, 114*, 40-48. https://doi.org/10.1016/j.cemconres.2017.02.009

Provis, J. L., & van Deventer, J. S. J. (2014). *Alkali-activated materials: State-of-the-art report, RILEM TC 224-AAM*. Springer. https://doi.org/10.1007/978-94-007-7672-2

Rangan, B. V. (2014). *Geopolymer concrete for environmental protection*. Faculty of Engineering, Curtin University.

Shi, C., Krivenko, P. V., & Roy, D. (2017). *Alkali-activated cements and concretes*. CRC Press.

Temuujin, J., van Riessen, A., & Williams, R. (2011). Influence of calcium compounds on the mechanical properties of fly ash geopolymer pastes. *Journal of Hazardous Materials, 167*(1-3), 82–88. https://doi.org/10.1016/j.jhazmat.2008.12.121

Tobie, F., Abo-El-Enein, S. A., & El-Hosiny, F. I. (2021). Effect of nano-silica on the properties of alkali-activated materials. *Construction and Building Materials, 271*, Article 121527. https://doi.org/10.1016/j.conbuildmat.2020.121527

Zhao, R., Xiao, N., Liu, Y., Zhan, W., & Wu, Z. (2024). Study on extraction of silica from rice husk by sol-gel method and its application in catalytic decomposition of methane. *Biomass Conversion and Biorefinery, 14*(9), 10067–10083. https://doi.org/10.1007/s13399-022-03524-4